Dalton Transactions

Accepted Manuscript

ROYAL SOCIETY OF CHEMISTRY

www.rsc.org/dalton

Efficient elimination of caffeine from water using Oxone activated by a magnetic and recyclable cobalt/carbon nanocomposite derived from ZIF-67

*Kun-Yi Andrew Lin** *and Bo-Chau Chen*

Department of Environmental Engineering, National Chung Hsing University,

250 Kuo-Kuang Road, Taichung, Taiwan, R.O.C.

*Corresponding Author. Tel: +886-4-22854709, E-mail address: linky@nchu.edu.tw

(Kun-Yi Andrew Lin)

Abstract

To eliminate caffeine, one of the most common pharmaceuticals and personal care products, from water, Oxone (peroxymonosulfate salt) was proposed to degrade caffeine. To accelerate the generation of sulfate radicals from Oxone, a magnetic cobalt/carbon nanocomposite (CCN) was prepared from a one-step carbonization of a cobalt-based Zeolitic Imidazolate Framework (ZIF-67). The resultant CCN exhibits immobilized cobalt and increased porosity, and can be magnetically manipulated. These characteristics make CCN a promising heterogeneous catalyst to activate Oxone for caffeine degradation. Factors affecting the caffeine degradation were investigated, including CCN loading, Oxone dosage, temperature, pH, surfactants, salt and inhibitors. Higher CCN loading, Oxone dosage and temperature greatly improved the caffeine degradation by CCN-activated Oxone. The acidic condition was also preferable over the basic condition for caffeine degradation. The addition of cetyltrimethylammonium bromide (CTAB) and NaCl both significantly hindered caffeine degradation because bromide from CTAB and chloride from NaCl scavenged sulfate radicals. Based on the effects of inhibitors (*i.e.*, methanol and *tert*-butyl alcohol), the caffeine degradation by CCN-activated Oxone was considered to primarily involve sulfate radicals and, less commonly, hydroxyl radicals. The intermediates generated during the caffeine degradation were analyzed using GC-MS and a possible degradation pathway was proposed. CCN was also able to activate Oxone for caffeine degradation for multiple cycles without changing its catalytic activity. These features reveal that CCN is an effective and promising catalyst for activation of Oxone for the degradation of caffeine.

Keywords: caffeine, Oxone, ZIF-67, cobalt, carbon

1. Introduction

Because of the widespread use of pharmaceuticals and personal care products (PPCPs), the high concentration of PPCPs can be detected in sewage treatment plant (STP) effluents [1], surface water [2, 3], and even groundwater [4]. PPCPs in the environment may be highly resistant to natural degradation and potentially toxic, and leading to adverse effects on ecology and human health [5]. Therefore, it is necessary to remove PPCPs from water, including STP effluents. Among numerous PPCPs, caffeine is one of the most common pharmaceuticals owing to its extensive usage in food and beverage [6]. Caffeine is also a common medicine to treat headaches and migraines [7, 8]. Although caffeine can be metabolized by humans, disposal of coffee and caffeinated beverages constitutes a major source of caffeine in sewerage [9]. Because caffeine exhibits a high solubility (*i.e.*, 37.5 g L^{-1} [10]), a low volatility and a high persistency to natural degradation, it can be easily found in STP influents and effluents, water supply and even drinking water [11].

To date, a number of methods have been proposed to remove caffeine from water, including adsorption [12, 13], biological treatment [14] and Advanced Oxidation Processes (AOPs). AOPs are particularly preferable because they can satisfactorily degrade refractory and non-biodegradable organic contaminants in a relatively short time using highly reactive oxygenic species such as ozone, hydroxyl and sulfate radicals. Rosal *et al.* successfully demonstrated the use of ozone to degrade caffeine [15], whereas Klamerth *et al.* [16] and Trovó *et al.* [17] employed Fenton reactions to generate hydroxyl radicals for the degradation of caffeine. While ozone and Fenton reactions were shown to eliminate caffeine, AOPs involving sulfate radicals (*e.g.*, $SO_4^{\bullet-}$) have also drawn great attention because sulfate radicals exhibit a high oxidation potential (2.5−3.1 V vs NHE) [18] and relatively long half-life periods (*i.e.*, 30−40 μs)

[19, 20]. To obtain sulfate radicals, Oxone (*i.e.*, potassium peroxymonosulfate salt) is increasingly used because it is commercially available and environmentally-friendly [21]. Nevertheless, catalysts are usually required in order to accelerate the generation of sulfate radicals from Oxone because of the slow self-activation of Oxone [21-28]. Generally, cobalt-based catalysts are considered as the most effective catalysts for the activation of Oxone [26, 28]. Therefore, Guo *et al.* used cobalt sulfate to activate Oxone for the degradation of caffeine [29]. However, the direct addition of cobalt ions may pose a risk in the event that cobalt ions cannot be recovered, remaining in aqueous solutions and leading to secondary contamination. To avoid the direct addition of cobalt ions, Qi *et al.* immobilized cobalt ions on a mesoporous silica support (*i.e.*, MCM-41) [30, 31]. The immobilization technique indeed prevented the direct addition of cobalt to solutions; however the recovery of catalysts still remains as an issue, especially in a large-scale operation. Additionally, the preparation of such a mesoporous support (*i.e.*, MCM-41) requires a long time because it involves hydrothermal processing. Therefore, development of an easy-to-recover and simple-to-prepare cobalt-based heterogeneous catalyst is desired.

To this end, we proposed to obtain a cobalt-based catalyst derived from Zeolitic Imidazolate Frameworks (ZIFs). ZIFs represent a special class of Metal Organic Frameworks (MOFs) owing to their zeolitic structures [32] and exceptional stability [33]. As MOFs recently are used as precursors to prepare nanoporous metal oxides [34-36] and carbonaceous composites [37-43], ZIFs, consisting of metals and organic ligands, are considered as ideal precursors for preparation of metal/carbon hybrid materials.

In this study, a cobalt-based ZIF (*i.e.*, ZIF-67) is selected and carbonized, because ZIF-67 can be simply prepared with a high yield in a relatively short time (*e.g.*, 2-4 h) using water as a solvent at room temperature [44]. ZIF-67 was first reported by Yaghi *et al.* [45] in 2008, and it exhibits a sodalite topology, consisting of cobalt as the metal center and 2-methylimidazole (2-MIM) as the ligand.

After a one-step carbonization, the cobalt content in ZIF-67 enables the resultant cobalt/carbon nanocomposite (CCN) to be controlled magnetically. The original hierarchical structure of ZIF-67 also renders CCN porous even after the carbonization. Therefore, the cobaltic, magnetic and porous CCN is a promising catalyst to activate Oxone for the degradation of caffeine.

In this study, CCN was prepared via the direct carbonization of ZIF-67 crystals and its morphology was determined using scanning electronic microscopy (SEM). The chemical composition was characterized using X-ray diffraction (XRD), FT-IR, Raman spectroscopy and X-photoelectron spectroscopy (XPS). Physical properties, such as thermogravimetric (TG) analysis, surface area and porosity, and magnetization, were also determined. Factors influencing the caffeine degradation were examined, including CCN loading, Oxone dosage, temperature, pH, co-existing ions, salt and inhibitors. Intermediates generated during the degradation of caffeine using CCN-activated Oxone were also determined by GC-MS and a possible degradation pathway was proposed. To evaluate recyclability of CCN, a multi-cycle test of degradation of caffeine was conducted without regeneration treatments on CCN.

2. Experimental

2.1 Materials

Chemicals used in this study were commercially available and used without purification. Caffeine, 2-methylimidazole (2-MIM), Oxone (peroxymonosulfate content: 44.7 wt%), and sodium dodecyl sulfate (SDS) were obtained from Sigma-Aldrich (USA). Cobalt nitrate was purchased from Choneye Pure Chemicals (Taiwan). Methanol was purchased from Merck (Germany), whereas *tert*-butyl alcohol was obtained from Alfa Aesar (USA). Cetyltrimethylammonium bromide (CTAB) was purchased from Acros Organics (USA). Deionized (DI) water was prepared to less than 18 MOhm-cm.

2.2 Preparation of Cobalt/Carbon Nanocomposite (CCN)

CCN was prepared based on the scheme illustrated as Fig. 1a. First, ZIF-67 crystals were synthesized by coordinating $Co(NO_3)_2$ with 2-MIM [44]. In a typical synthesis, 8 mmol of $Co(NO_3)_2$ was added to 100 mL of DI water and 32 mmol of 2-MIM was added to another 100 mL of DI water. Next, the cobalt solution was slowly poured into the solution of 2-MIM and the mixture was stirred at ambient temperature for 4 h. The precipitate was collected via centrifugation and washed thoroughly with DI water. The as-synthesized crystals were dried in a vacuum oven 100 °C for 8 h to obtain ZIF-67 crystals.

The resulting ZIF-67 crystals were placed into a tubular furnace and carbonized in nitrogen at 600 °C for 4 h to yield black-colored particles. These particles were then washed with ethanol thoroughly and oven-dried at 85 °C for 8 h to obtain the final product, CCN.

2.3 Characterization of CCN

Characteristics of CCN and its precursor, ZIF-67, were first determined using a field-emission SEM (Zeiss UltraPlus, Germany) to observe their morphologies. Crystallinities of CCN and ZIF-67 were measured using an X-ray diffractometer (Bruker D8 Discover, USA) with copper as an anode material (40 mA, 35 kV). IR spectroscopic analysis of CCN was conducted using a Fourier-Transform IR spectrometer (Horiba FT-730, Japan) with KBr pellets.

Raman spectroscopy was also employed to investigate composition of conjugated carbon in CCN using a Raman spectrometer (Tokyo Instruments Inc. Nanofinder, Japan). The cobalt content within CCN was further identified by X-ray Photoelectron Spectroscopy (XPS) with Versa Probe/Scanning ESCA Microprobe (PHI 5000, ULVAC-PHI, Inc., Japan). The magnetic property of CCN was determined by measuring magnetization under a varied magnetic field using a SQUID Vibrating Sample Magnetometer (Quantum Design MPMS, USA) at 27 °C. Thermogrametric (TG) analyses of CCN and ZIF-67 were obtained using a thermogravimetric analyzer (ISI TGA i1000, USA) at a heating rate of 20 °C min^{-1} from 20 to 800 °C with nitrogen or air as a carrier gas. Surface area and porosity of CCN and its precursor, ZIF-67, were obtained by measuring their N_2 sorption/desorption isotherms after CCN and ZIF-67 were degassed at 120 °C for 24 h using a volumetric gas adsorption analyzer (Micromeritics ASAP 2020, USA).

2.4 Elimination of Caffeine in water using Oxone activated by CCN

Elimination of caffeine using Oxone was conducted by batch-type experiments. Typically, 50 mg of Oxone powder was added to 0.2 L of caffeine solution with an initial concentration (C_0) of 50 mg L^{-1}. Upon the dissolution of Oxone, 10 mg of

CCN was added to the caffeine solution and the mixture was maintained at a certain temperature using a digital temperature-controllable stirring plate. At pre-set times, samples aliquots were withdrawn from the batch reactor and the remaining concentration (C_t) at a given time was determined using a UV-Vis spectrophotometer at 275 nm (Hitachi U-2900 spectrometer). Total organic carbon (TOC) concentration of caffeine solutions during the degradation was determined by a total carbon analyzer (Shimadzu TOC-V, Japan) after quenching sample aliquots by sodium thiosulfate. To investigate roles of CCN and Oxone during the degradation, CCN loadings and Oxone dosages were varied: CCN loading was increased from 25 to 150 mg L^{-1} and Oxone dosage was increased from 25 to 250 mg L^{-1}. The solution temperature was also changed from 20 to 40 °C to examine the effect of temperature and to determine the activation energy of caffeine degradation. In addition, the initial pH of solution was adjusted to 3, 7 and 10 to investigate caffeine degradation using CCN-activated Oxone under acidic, neutral and basic conditions, respectively. The pH for the unadjusted experiment was 3.5. The influence of co-existing surfactants was examined by adding a common cationic surfactant, CTAB, and a typical anionic surfactant, SDS, to caffeine solutions. The effect of salt was also investigated by adding different amounts of a common salt, NaCl, to caffeine solutions.

Two radical-scavengers, methanol and TBA, were added to caffeine solutions to examine their inhibitive effects on the degradation and to provide insights into the degradation mechanism using CCN-activated Oxone process. To evaluate whether CCN serves as a durable and re-usable catalyst to activate Oxone, the spent CCN was recovered and used directly in multiple cycles of degradation experiment without regeneration treatments. The intermediate products were identified by GC-MS (Thermo Scientific DSQ II, USA) with a DB-5MS capillary column (30 m × 0.25mm

× 0.25 μm). Sample aliquots of the degradation of caffeine were quenched by methanol and the degradation products were extracted by dichloromethane (20 mL). The recovered organic phases were then condensed to around 2 mL at 60 °C. During the analysis of GC-MS, a temperature program was used as follows. An initial temperature was set to 50 °C and increased to 200 °C at increments of 50 °C min^{-1} and then held for 2 min. The temperature was then increased to 275 °C at increments of 30 °C min^{-1}.

3. Results and Discussion

3.1 Characterization of CCN

Before characterizing the morphology of CCN, it is necessary to determine the morphology of its precursor, ZIF-67. Fig. 1b shows a SEM image of ZIF-67 crystals which exhibited a well-defined sodalite structure with sharp edges and an average size of 682 (± 196) nm. The crystalline structure of ZIF-67 was also measured and is shown in the upper part of Fig. 2a. This structure can be readily indexed to the typical pattern of ZIF-67 [46], indicating that ZIF-67 crystals were well-developed. After the carbonization of ZIF-67, the morphology of the resultant CCN is displayed in Fig. 1c and the average size of CCN is 471 (± 134) nm. The original sodalite morphology of ZIF-67 had been concaved and shrunken due to the carbonization. Nevertheless, the edges of ZIF-67, although distorted, can still be observed in CCN. Fig. S1 reveals TEM images of CCN and its precursor, ZIF-67 (please see **ESI**†). It can be seen that before the carbonization, ZIF-67 exhibits very smooth morphology and no particles formed within ZIF-67 or on its surface. However, once ZIF-67 was carbonized to form CCN, small dark-colored cobalt oxide particles can be found quite evenly distributed within CCN, without significant aggregations. Fig. S1b also shows that

ZIF-67 crystals with different sizes can be converted to CCN particles which contain evenly-distributed cobalt oxide nanoparticles with an average size of 43 (± 12) nm. The crystalline structure of CCN is also shown in the lower part of Fig. 2a, in which no XRD pattern of ZIF-67 was preserved, indicating that ZIF-67 was transformed to another material. The XRD pattern of CCN can be indexed to cobalt oxide according to JCPDS card # 42-1467, indicating that cobalt oxide derived from ZIF-67 exhibited the spinel lattice structure. The average grain size of cobalt oxide is 4.6 nm based on the Debye-Scherrer equation using MDI Jade 5.

The presence of cobalt oxide can be also confirmed using spectroscopic analyses. Fig. 2b shows an IR spectrum of CCN, in which peaks at 570 and 661 cm^{-1} can be attributed to the stretching vibrations of Co-O bond. In particular, the peak at 661 cm^{-1} is considered the ABO_3 form of cobalt oxide, in which A represents cobalt located in the tetrahedral position and B denotes cobalt in the octahedral position [47]. On the other hand, the peak at 570 cm^{-1} represents the BOB_3 from of cobalt oxide in the spinel lattice. An additional peak at 1585 cm^{-1} can be assigned to the C-N bond derived from 2-MIM. Raman spectroscopic analysis (Fig. 2c) was also conducted to characterize CCN and a number of peaks at 192, 470, 510, 608 and 682 Raman shift (cm^{-1}) were also attributed to the cobalt content of CCN [47]. The conjugated carbon of CCN was also revealed in the Raman spectra. The peaks at 1350 and 1590 Raman shift (cm^{-1}) correspond to disordered structure carbon (*i.e.*, the D band) and graphitic carbon (*i.e.*, the G band) of CCN, respectively. Fig. 2d shows the Co 2p core-level XPS spectrum, which further reveals the cobalt species of CCN. The peaks at 780.2 and 781.8 eV are considered as Co^{3+} and Co^{2+}, respectively [48, 49], whereas the peaks at 786.3 and 804.8 eV can be attributed to the shake-up satellite peaks of Co^{2+}

[49]. In addition, nitrogen derived from 2-MIM was found to remain within CCN as the N 1s core-level XPS spectrum reveals in Fig. S2 (see **ESI†**).

The magnetization property of CCN was also evaluated. Fig. 3a shows the magnetization as a function of magnetic field; the magnetization approached a saturation of 45 emu g^{-1}, indicating that CCN is a magnetic material. Fig. 3b demonstrates that CCN could be well-dispersed in water to form a stable suspension and CCN nanoparticles can be easily collected/recovered using an external magnet.

The thermogravimetric (TG) analysis of CCN is seen in Fig. S3 (see **ESI†**), including the TG curve of ZIF-67. The TG curve of ZIF-67 in N_2 started at 200 °C owing to the decomposition of 2-MIM [50]. The TG curve continued to decrease until 500 °C and then remained stable at 20 wt% afterwards. This suggests that each gram of ZIF-67 can be converted to 0.2 g of CCN. Once ZIF-67 was converted to CCN, the thermal stability of CCN was quite stable and only slight weight loss was observed in CCN during the TG decomposition in N_2 up to 800 °C. The TG decomposition of CCN in air was also examined and the weight decreased to 50 wt% after 250 °C, indicating that carbon accounted for around 50 wt% of the entire CCN.

To demonstrate the variation of the textural property from ZIF-67 to CCN, N_2 sorption and desorption isotherms of ZIF-67 and CCN are provided in Fig. S4a and Fig. S5a, respectively. While the isotherm curve of ZIF-67 is a typical IUPAC type I sorption, the isotherm curve of CCN represents a combination of the IUPAC type I and II sorption types. This suggests that ZIF-67 primarily exhibits micropores as revealed in Fig. S4b, whereas CCN might exhibit macroporous structures as shown in Fig. S5b. As a result, the BET surface area and porosity of CCN (*i.e.*, 220 m^2 g^{-1} and 0.34 cm^3 g^{-1}, respectively) were much lower than those of ZIF-67 (*i.e.*, 1717 m^2 g^{-1} and 0.7 cm^3 g^{-1}, respectively). Nevertheless, the pore size distribution of CCN (Fig.

S5b) reveals that CCN was comprised of mesopores with a small portion of micropores, indicating that the porosity of CCN remained even after carbonization.

3.2 Elimination of caffeine in water by CCN-activated Oxone

Since ZIF-8, an isostructural ZIF to ZIF-67, had been reported to adsorb caffeine in solutions [51], it was necessary to examine whether caffeine could be removed from water via adsorption prior to investigating the degradation of caffeine using CCN-activated Oxone. Fig. 4a shows the concentration of caffeine as a function of time in the presence of CCN alone, and no caffeine was removed, suggesting that CCN did not exhibit strong affinity toward caffeine. The elimination of caffeine in the presence of Oxone was shown in Fig. 4a. While Oxone alone was capable of eliminating caffeine, C_t/C_0 did not approach 0.6 after 120 min. This suggests that Oxone alone was ineffective without activation by catalysts. Once CCN was added to the caffeine solution containing Oxone, C_t/C_0 reached 0.2 in 60 min and approached 0 in 120 min. The UV-Vis spectral variation of the caffeine solution (Fig. S6a, see **ESI**†) also reveals that caffeine was gradually eliminated from water. This indicates that the combination of CCN and Oxone significantly improved the degradation of caffeine.

Considering the existence of both Co^{3+} and Co^{2+} as revealed in the XPS analysis, either cation could react with Oxone to convert peroxymonosulfate anion (HSO_5^-) to sulfate radicals as illustrated in Fig. S7 according to the following equations (Eqs.(1)-(3)) [39, 52-57]:

$$Co^{2+} + HSO_5^- \rightarrow Co^{3+} + SO_4^{\bullet-} + OH^- \quad (1)$$

$$Co^{3+} + HSO_5^- \rightarrow Co^{2+} + SO_5^{\bullet-} + H^+ \quad (2)$$

$$2\ SO_5^{\bullet-} \rightarrow 2\ SO_4^{\bullet-} + O_2 \quad (3)$$

The high oxidation potential of $SO_4^{\bullet-}$ (*i.e.*, 2.5−3.1 V vs NHE) could attack caffeine, causing degradation and mineralization. This can be validated by a decrease of total organic carbon (TOC) concentration of the caffeine solution (Fig. S6b, see **ESI†**) during the degradation experiment.

3.3 Effects of CCN loading and Oxone dosage on the elimination of caffeine

CCN loading and Oxone dosage were varied to examine their respective effects on the elimination of caffeine. Fig. 4b shows degradation curves using CCN loadings of 25, 50 and 150 mg L^{-1} while Oxone dosage was fixed at 250 mg L^{-1}. A distinct trend can be observed: a higher CCN loading significantly accelerated the degradation kinetics. Another noteworthy observation is that even though CCN loading was as low as 25 mg L^{-1}, C_t/C_0 still approached 0 in 120 min This indicates that CCN was a highly effective catalyst to activate Oxone. To quantitatively evaluate the enhancement in degradation kinetics at a higher CCN loading, the degradation kinetics was analyzed by a common rate law, the pseudo first order equation, as follows (Eq. (4)):

$$C_t = C_0 \exp(-k_1 t) \qquad (4)$$

where k_1 is the first order rate constant of the degradation. While CCN loading was increased from 25 to 150 mg L^{-1}, k_1 changed from 0.0208 to 0.1000 min^{-1}, almost a five-fold increase. This validates that a higher CCN loading substantially accelerated the degradation kinetics.

Fig. 4c shows the effect of Oxone dosage on the caffeine degradation. A higher Oxone dosage indeed improved the caffeine degradation as C_t/C_0 almost reached 0 in 60 min using Oxone = 250 mg L^{-1}. The kinetics at a higher Oxone dosage was also accelerated. When Oxone was increased from 150 to 250 mg L^{-1}, k_1 rose from 0.0256 to 0.0421 min^{-1}. However, when Oxone = 25 mg L^{-1}, C_t/C_0 merely approached 0.6

and k_1 became 0.0157 min^{-1}, suggesting that a sufficient Oxone dosage was necessary to effectively degrade caffeine.

3.4 Effects of temperature and pH on caffeine degradation

The effect of temperature was also investigated by changing the temperature of caffeine solutions from 20 to 40 °C. When the temperature was increased from 20 to 30 °C, the kinetics became much faster and C_t/C_0 reached a lower value (Fig. 4d), indicating the positive effect of a higher temperature. The k_1 value was also increased, from 0.0256 to 0.0520 min^{-1}. Similarly, when temperature was increased to 40 °C, k_1 increased to 0.1364 min^{-1}, demonstrating the remarkable effect of higher temperature on the degradation of contaminants as reported in previous studies [25].

Rate constants can typically be associated with temperature via the Arrhenius equation as follows (Eq.(5)):

$$\ln k_1 = \ln k - E_a/RT \quad (5)$$

where E_a is the activation energy (kJ mol–1); k represents the temperature-independent factor (g mg^{-1} min^{-1}); R is the universal gas constant; and T is the solution temperature in Kelvin (K). Thus, the activation energy of caffeine degradation using CCN-activated Oxone can be determined by the Arrhenius equation. To do so, a plot of $1/T$ versus ln k_1 was drawn in Fig. S8 (see **ESI**†). One can observe that the data points of k_1 values at different temperatures are well fitted by a linear regression with $R^2 = 0.993$. Based on the slope of the fitting line, the activation energy was estimated to be 64.5 kJ mol^{-1}.

The effect of pH was investigated by changing the initial pH of caffeine solutions to 3, 7 and 10, corresponding to acidic, neutral and basic conditions,

respectively. Degradation at the unadjusted initial pH (*i.e.*, 3.5) was also included in Fig. 5a for comparison. The degradation of caffeine at pH = 3 was almost the same as that at the unadjusted pH. The k_1 value obtained at pH = 3 was 0.0270 min^{-1} (Table 1), quite similar to k_1 at the unadjusted pH (*i.e.*, .0256 min^{-1}). On the other hand, the caffeine degradation was slightly hindered when pH was raised to 7; C_t/C_0 reached just 0.4 in 120 min and k_1 was 0.0104 min^{-1}. The adverse effect on the caffeine degradation was even more pronounced when pH was increased to 10. At pH = 10, C_t/C_0 did not even reach 0.9 in 120 min with k_1 = 0.0030 min^{-1}. These results indicate that the caffeine degradation by CCN-activated Oxone was not significantly influenced under the acidic condition, possibly owing to the fact that Oxone is relatively stable at low pH [54]. Besides, Oxone is also considered as an acidic oxidant and thus the generation of $SO_4^{\bullet-}$ can be also facilitated at low pH values [31]. This could be a possible reason for the slightly higher k_1 obtained at pH = 3 (*i.e.*, 0.0270 min^{-1}) than that obtained at the unadjusted pH (*i.e.*, 0.0256 min^{-1}). In contrast, Oxone under basic conditions was prone to decompose without producing sulfate radicals [54, 58, 59] and therefore decreased the degradation extent and kinetics. Another possibility is that the surface of CCN might be negatively-charged owing to the residence of hydroxyl ions under the basic condition. As a result, the contact between the negatively-charged CCN and $SO_5^{\bullet-}$, which is an efficient species for the generation of $SO_4^{\bullet-}$, might be limited. This could lead to a reduced yield of $SO_4^{\bullet-}$ and less degradation of caffeine [31].

3.5 Effects of co-existing ions on caffeine degradation

A number of studies have reported that caffeine and surfactants can be simultaneously detected in septic tank effluents [60], drinking water wells and groundwater [61]. Therefore, it is necessary to examine whether CCN-activated Oxone could be still capable of degrading caffeine in the presence of other contaminants, such as surfactants. Additionally, because wastewater typically also contain salts [62], the effect of different concentrations of salt on the degradation efficiency of CCN-activated Oxone was evaluated. Fig. 5b shows the caffeine degradation in the presences of two widely-employed surfactants, CTAB and SDS. When CTAB, a typical cationic surfactant, was added in the caffeine solution, C_t/C_0 slowly approached 0.5. Bromide-comprising CTAB has been proven to be a radical scavenger that react with sulfate radicals to form bromine radicals and bromate as follows (Eqs.(6)-(12)) [63, 64]:

$$Br^- + SO_4^{\bullet -} \rightarrow Br^{\bullet} + SO_4^{2-} \qquad k = 3.5 \times 10^9\ M^{-1}\ s^{-1} \qquad (6)$$

$$Br^{\bullet} + Br^- \rightarrow Br_2^{\bullet -} \qquad k = 1.2 \times 10^{10}\ M^{-1}\ s^{-1} \qquad (7)$$

$$Br_2^{\bullet -} + Br^{\bullet} \rightarrow Br_2 + Br^- \qquad k = 2.0 \times 10^9\ M^{-1}\ s^{-1} \qquad (8)$$

$$Br_2^{\bullet -} + Br_2^{\bullet -} \rightarrow Br_2 + 2Br^- \qquad k = 1.9 \times 10^9\ M^{-1}\ s^{-1} \qquad (9)$$

$$Br^{\bullet} + Br^{\bullet} \rightarrow Br_2 \qquad k = 1.0 \times 10^9\ M^{-1}\ s^{-1} \qquad (10)$$

$$Br_2 + H_2O \rightarrow HBrO + H^+ + Br^- \qquad k = 1.6 \times 10^{10}\ M^{-1}\ s^{-1} \qquad (11)$$

$$HBrO + SO_4^{\bullet -} \rightarrow BrO_3^- \qquad (12)$$

The degradation of caffeine was slightly affected in the presence of SDS, a typical anionic surfactant. SDS, consisting of a long alkyl chain, might also react with sulfate and hydroxyl radicals, thereby consuming a portion of the radicals generated from CCN-activated Oxone. It should be noted that the concentration of SDS added to the solution was equivalent to caffeine (*i.e.*, 50 mg L^{-1}). However, the decrease in the

degradation of caffeine was not significant, implying that CCN-activated Oxone exhibited a higher selectivity toward the degradation of caffeine over SDS.

The effect of salt was also investigated and is shown in Fig. 6a. NaCl was selected as a model salt which was added to caffeine solutions during the degradation. As the concentration of NaCl increased, the extent of caffeine degradation gradually decreased. Thus, the presence of NaCl inhibited the caffeine degradation. Similar to bromide ions, chloride ions could also react with $SO_4^{\bullet-}$ to generate chlorine radicals and therefore the addition of NaCl might scavenge the sulfate radicals, thereby hindering the caffeine degradation as follows (Eqs.(13)-(14)) [31]:

$$Cl^- + SO_4^{\bullet-} \rightarrow Cl^{\bullet} + SO_4^{2-} \quad k_f = 3.2 \times 10^8\ M^{-1}\ s^{-1};\ k_r = 2.1 \times 10^8\ M^{-1}\ s^{-1} \qquad (13)$$

$$Cl^{\bullet} + Cl^- \rightarrow Cl_2^{\bullet-} \quad k_f = 7.8 \times 10^9\ M^{-1}\ s^{-1};\ k_r = 5.7 \times 10^4\ M^{-1}\ s^{-1} \qquad (14)$$

3.6 Effects of inhibitors on caffeine degradation

A few radical scavengers were also evaluated for their inhibitive effects on the caffeine degradation by CCN-activated Oxone. Investigations of the inhibitive effect of particular scavengers could also provide insights into the mechanism for caffeine degradation. First, *tert*-butyl alcohol (TBA) was used as a probe reagent specifically for hydroxyl radicals ($OH^{\bullet}$). Fig. 6b shows that the caffeine degradation was affected as C_t/C_0 approached around 0.1 in 120 min and k_1 became 0.0415 min^{-1}. This indicates that TBA slightly inhibited the caffeine degradation and the degradation mechanism seemed to involve hydroxyl radicals, which could be derived from a reaction between sulfate radicals and H_2O as follows (Eq. (15))[65]:

$$SO_4^{-\bullet} + H_2O \rightarrow SO_4^{2-} + OH^{\bullet} + H^+ \qquad (15)$$

Subsequently, methanol was used as an inhibitor since it is a probe reagent for both sulfate and hydroxyl radicals. In the presence of methanol (Fig. 6b), degradation was

substantially hindered; C_t/C_0 did not reach 0.8 in 120 min and k_1 decreased to a mere 0.0011 min^{-1}. This suggests that the degradation mechanism for caffeine by CCN-activated Oxone primarily involves sulfate radicals and, to a less extent, hydroxyl radicals.

3.7 A proposed degradation pathway for caffeine by CCN-activated Oxone

To further investigate the degradation pathway of caffeine using CCN-activated Oxone process, GC-MS was employed to determine the transformation of caffeine and possible intermediates during the degradation. Five intermediates were detected and shown as P1-P5 in Fig. S9 (see **ESI**†). The proposed caffeine degradation pathway by CCN-activated Oxone based on the detected intermediates is shown in Fig. 7. When caffeine was added to water, a hydroxylated form of caffeine might initially occur as C1 in Fig. 7 [15]. Subsequently, $SO4^{\bullet-}$ and $OH^{\bullet}$ could attack the C-N bond of the 5-member ring to prompt a ring-opening reaction, generating an intermediate P1. Via the further oxidation, P1 could be degraded to P2. Next, the C=C bond of caffeine could also be attacked by $SO4^{\bullet-}$ and $OH^{\bullet}$, opening the six-member ring and leading to the formation of another intermediate, C2, consisting of two carbonyl groups with nitrogen functional groups. The carbonyl groups might be attacked by the radicals and detached from C2 to form P3, which was *N*-acetyl-*N*-methylacetamide ($C_5H_9NO_2$) with a carbonyl group and a secondary amine group. P3 could be further oxidized and the methyl group of the secondary amine group was attacked to form P4. Starting from P4, a few intermediates might form simultaneously such as P5-1 and P5-2. P5-1 could be derived from P4 by transforming the carbonyl group to a methyl group. P5-2 might occur when the

methyl group was further oxidized and the primary amine group was oxidized and replaced by a hydroxyl group [30].

3.8 The recyclability of CCN to activate Oxone

As a heterogeneous catalyst, the recyclability of CCN for activating Oxone for the caffeine degradation is an important aspect. Thus, we conducted a multiple cycle test using CCN to activate Oxone for caffeine degradation. The used CCN was collected using a permanent magnet and added to the subsequent experiment without any regeneration treatments. Fig. 8 shows the efficiency of caffeine degradation for 5 cycles; the efficiency remained almost the same over 5 cycles even though CCN was not regenerated. This indicates that CCN is a recyclable, stable and effective heterogeneous and magnetic catalyst for activating Oxone.

4. Conclusions

In this study, the magnetic cobalt/carbon nanocomposite (CCN) was prepared from the one-step carbonization of ZIF-67. CCN is characterized by immobilized cobalt, porosity and magnetic controllability; these features suggest that CCN is a promising heterogeneous catalyst to activate Oxone for the degradation of caffeine. Higher CCN loading, Oxone dosage and temperature were found to greatly improve the caffeine degradation by CCN-activated Oxone. The acidic condition was preferable over the basic condition for caffeine degradation. In addition, the presence of other contaminants, such as surfactants, may decrease the efficiency of CCN. Based on the effects of such inhibitors, caffeine degradation by CCN-activated Oxone primarily involves sulfate radicals as well as hydroxyl radicals to some extent. The intermediates generated during caffeine degradation were also analyzed and a possible

degradation pathway was proposed. CCN was also able to activate Oxone for caffeine degradation over multiple cycles without changing its catalytic activity. These findings reveal that CCN appears to be an effective and promising catalyst for activation of Oxone for the degradation of caffeine.

Acknowledgment

The authors thank Andrew P. Jochems at New Mexico Bureau of Geology & Mineral Resources (Socorro, New Mexico, USA) and Spyros Schismenos at National Yunlin University of Science and Technology (Taiwan) for their suggestions on the English writing. The authors also want to acknowledge the assistance from Research Center for Sustainable Energy and Nanotechnology at National Chung Hsing University on the material characterization. This study is supported by Ministry of Science and Technology of Taiwan (MOST 104-2221-E-005-007-MY2).

References:

[1] J. Martín, M.D. Camacho-Muñoz, J.L. Santos, I. Aparicio, E. Alonso, Distribution and temporal evolution of pharmaceutically active compounds alongside sewage sludge treatment. Risk assessment of sludge application onto soils, Journal of Environmental Management, 102 (2012) 18-25.

[2] V. Matamoros, C.A. Arias, L.X. Nguyen, V. Salvadó, H. Brix, Occurrence and behavior of emerging contaminants in surface water and a restored wetland, Chemosphere, 88 (2012) 1083-1089.

[3] M. Lahti, A. Oikari, Vertical distribution of pharmaceuticals in lake sediments—citalopram as potential chemomarker, Environmental Toxicology and Chemistry, 31 (2012) 1738-1744.

[4] X. Peng, W. Ou, C. Wang, Z. Wang, Q. Huang, J. Jin, J. Tan, Occurrence and ecological potential of pharmaceuticals and personal care products in groundwater and reservoirs in the vicinity of municipal landfills in China, Sci. Total Environ., 490 (2014) 889-898.

[5] W. Zhang, M. Zhang, K. Lin, W. Sun, B. Xiong, M. Guo, X. Cui, R. Fu, Eco-toxicological effect of Carbamazepine on Scenedesmus obliquus and Chlorella pyrenoidosa, Environmental Toxicology and Pharmacology, 33 (2012) 344-352.

[6] C.A. Knight, I. Knight, D.C. Mitchell, J.E. Zepp, Beverage caffeine intake in US consumers and subpopulations of interest: estimates from the Share of Intake Panel survey, Food and Chemical Toxicology, 42 (2004) 1923-1930.

[7] F.J. Karle Iii, P.S. Auerbach, Migraine Headache Confounding the Diagnosis of Acute Mountain Sickness, Wilderness & Environmental Medicine, 25 (2014) 60-68.

[8] T.J. Schwedt, Migraine, Medication Overuse Headache and, in: M.J. Aminoff, R.B. Daroff (Eds.) Encyclopedia of the Neurological Sciences (Second Edition), Academic Press, Oxford, 2014, pp. 53-57.

[9] F.J. Beltrán, A. Aguinaco, J.F. García-Araya, Application of Ozone Involving Advanced Oxidation Processes to Remove Some Pharmaceutical Compounds from Urban Wastewaters, Ozone: Science & Engineering, 34 (2012) 3-15.

[10] P. Sriamornsak, R.A. Kennedy, Effect of drug solubility on release behavior of calcium polysaccharide gel-coated pellets, European Journal of Pharmaceutical Sciences, 32 (2007) 231-239.

[11] F. Sodré, M. Locatelli, W. Jardim, Occurrence of Emerging Contaminants in Brazilian Drinking Waters: A Sewage-To-Tap Issue, Water Air Soil Pollut, 206 (2010) 57-67.

[12] J.L. Sotelo, G. Ovejero, A. Rodríguez, S. Álvarez, J. Galán, J. García, Competitive adsorption studies of caffeine and diclofenac aqueous solutions by activated carbon, Chemical Engineering Journal, 240 (2014) 443-453.

[13] J. Sotelo, G. Ovejero, A. Rodríguez, S. Álvarez, J. García, Study of Natural Clay Adsorbent Sepiolite for the Removal of Caffeine from Aqueous Solutions: Batch and Fixed-Bed Column Operation, Water, Air, & Soil Pollution, 224 (2013) 1-15.

[14] M. Kim, P. Guerra, A. Shah, M. Parsa, M. Alaee, S.A. Smyth, Removal of pharmaceuticals and personal care products in a membrane bioreactor wastewater treatment plant, Water Science & Technology 69 (2014) 2221–2229.

[15] R. Rosal, A. Rodríguez, J.A. Perdigón-Melón, A. Petre, E. García-Calvo, M.J. Gómez, A. Agüera, A.R. Fernández-Alba, Degradation of caffeine and identification of the transformation products generated by ozonation, Chemosphere, 74 (2009) 825-831.

[16] N. Klamerth, N. Miranda, S. Malato, A. Agüera, A.R. Fernández-Alba, M.I. Maldonado, J.M. Coronado, Degradation of emerging contaminants at low concentrations in MWTPs effluents with mild solar photo-Fenton and TiO2, Catalysis Today, 144 (2009) 124-130.

[17] A.G. Trovó, T.F.S. Silva, O. Gomes Jr, A.E.H. Machado, W.B. Neto, P.S. Muller Jr, D. Daniel, Degradation of caffeine by photo-Fenton process: Optimization of treatment conditions using experimental design, Chemosphere, 90 (2013) 170-175.

[18] P. Neta, R.E. Huie, A.B. Ross, Rate Constants for Reactions of Inorganic Radicals in Aqueous Solution, Journal of Physical and Chemical Reference Data, 17 (1988) 1027-1284.

[19] T. Olmez-Hanci, I. Arslan-Alaton, Comparison of sulfate and hydroxyl radical based advanced oxidation of phenol, Chemical Engineering Journal, 224 (2013) 10-16.

[20] E.G. Janzen, Y. Kotake, H. Randall D, Stabilities of hydroxyl radical spin adducts of PBN-type spin traps, Free Radical Biology and Medicine, 12 (1992) 169-173.

[21] P. Hu, M. Long, Cobalt-catalyzed sulfate radical-based advanced oxidation: A review on heterogeneous catalysts and applications, Applied Catalysis B: Environmental, 181 (2016) 103-117.

[22] G.P. Anipsitakis, E. Stathatos, D.D. Dionysiou, Heterogeneous Activation of Oxone Using Co3O4, The Journal of Physical Chemistry B, 109 (2005) 13052-13055.

[23] G. Wei, X. Liang, Z. He, Y. Liao, Z. Xie, P. Liu, S. Ji, H. He, D. Li, J. Zhang, Heterogeneous activation of Oxone by substituted magnetites Fe3−xMxO4 (Cr,

Mn, Co, Ni) for degradation of Acid Orange II at neutral pH, Journal of Molecular Catalysis A: Chemical, 398 (2015) 86-94.

[24] L. Hu, F. Yang, W. Lu, Y. Hao, H. Yuan, Heterogeneous activation of oxone with CoMg/SBA-15 for the degradation of dye Rhodamine B in aqueous solution, Applied Catalysis B: Environmental, 134–135 (2013) 7-18.

[25] K.-Y.A. Lin, H.-A. Chang, R.-C. Chen, MOF-derived magnetic carbonaceous nanocomposite as a heterogeneous catalyst to activate oxone for decolorization of Rhodamine B in water, Chemosphere, 130 (2015) 66-72.

[26] Q. Yang, H. Choi, S.R. Al-Abed, D.D. Dionysiou, Iron–cobalt mixed oxide nanocatalysts: Heterogeneous peroxymonosulfate activation, cobalt leaching, and ferromagnetic properties for environmental applications, Applied Catalysis B: Environmental, 88 (2009) 462-469.

[27] S. Yang, P. Wang, X. Yang, L. Shan, W. Zhang, X. Shao, R. Niu, Degradation efficiencies of azo dye Acid Orange 7 by the interaction of heat, UV and anions with common oxidants: Persulfate, peroxymonosulfate and hydrogen peroxide, Journal of Hazardous Materials, 179 (2010) 552-558.

[28] C. Cai, H. Zhang, X. Zhong, L. Hou, Ultrasound enhanced heterogeneous activation of peroxymonosulfate by a bimetallic Fe–Co/SBA-15 catalyst for the degradation of Orange II in water, Journal of Hazardous Materials, 283 (2015) 70-79.

[29] Y. Guo, T. Shen, C. Wang, J. Sun, X. Wang, Rapid removal of caffeine in aqueous solutions by peroxymonosulfate oxidant activated with cobalt ion, Water Science & Technology, 72 (2015) 478–483.

[30] F. Qi, W. Chu, B. Xu, Catalytic degradation of caffeine in aqueous solutions by cobalt-MCM41 activation of peroxymonosulfate, Applied Catalysis B: Environmental, 134–135 (2013) 324-332.

[31] F. Qi, W. Chu, B. Xu, Modeling the heterogeneous peroxymonosulfate/Co-MCM41 process for the degradation of caffeine and the study of influence of cobalt sources, Chemical Engineering Journal, 235 (2014) 10-18.

[32] A. Phan, C.J. Doonan, F.J. Uribe-Romo, C.B. Knobler, M. O'Keeffe, O.M. Yaghi, Synthesis, Structure, and Carbon Dioxide Capture Properties of Zeolitic Imidazolate Frameworks, Accounts of Chemical Research, 43 (2010) 58-67.

[33] K.S. Park, Z. Ni, A.P. Côté, J.Y. Choi, R. Huang, F.J. Uribe-Romo, H.K. Chae, M. O'Keeffe, O.M. Yaghi, Exceptional chemical and thermal stability of zeolitic imidazolate frameworks, Proceedings of the National Academy of Sciences of the United States of America, 103 (2006) 10186-10191.

[34] J.J. King, Inorganic persulfate cleaning solution for acoustic materials, in, Google Patents, 1983.

[35] Y. Song, X. Li, C. Wei, J. Fu, F. Xu, H. Tan, J. Tang, L. Wang, A Green Strategy to Prepare Metal Oxide Superstructure from Metal-Organic Frameworks, Scientific Reports, 5 (2015) 8401.

[36] T.K. Kim, K.J. Lee, J.Y. Cheon, J.H. Lee, S.H. Joo, H.R. Moon, Nanoporous Metal Oxides with Tunable and Nanocrystalline Frameworks via Conversion of Metal–Organic Frameworks, Journal of the American Chemical Society, 135 (2013) 8940-8946.

[37] J. Hu, H. Wang, Q. Gao, H. Guo, Porous carbons prepared by using metal–organic framework as the precursor for supercapacitors, Carbon, 48 (2010) 3599-3606.

[38] A. Banerjee, R. Gokhale, S. Bhatnagar, J. Jog, M. Bhardwaj, B. Lefez, B. Hannoyer, S. Ogale, MOF derived porous carbon-Fe3O4 nanocomposite as a high performance, recyclable environmental superadsorbent, J. Mater. Chem., 22 (2012) 19694-19699.

[39] G. Zhang, C. Li, J. Liu, L. Zhou, R. Liu, X. Han, H. Huang, H. Hu, Y. Liu, Z. Kang, One-step conversion from metal-organic frameworks to Co3O4@N-doped carbon nanocomposites towards highly efficient oxygen reduction catalysts, Journal of Materials Chemistry A, 2 (2014) 8184-8189.

[40] G. Yu, J. Sun, F. Muhammad, P. Wang, G. Zhu, Cobalt-based metal organic framework as precursor to achieve superior catalytic activity for aerobic epoxidation of styrene, RSC Adv., 4 (2014) 38804-38811.

[41] N.L. Torad, M. Hu, S. Ishihara, H. Sukegawa, A.A. Belik, M. Imura, K. Ariga, Y. Sakka, Y. Yamauchi, Direct Synthesis of MOF-Derived Nanoporous Carbon with Magnetic Co Nanoparticles toward Efficient Water Treatment, Small, 10 (2014) 2096-2107.

[42] K.-Y. Andrew Lin, F.-K. Hsu, W.-D. Lee, Magnetic cobalt-graphene nanocomposite derived from self-assembly of MOFs with graphene oxide as an activator for peroxymonosulfate, Journal of Materials Chemistry A, 3 (2015) 9480-9490.

[43] K.-Y. Andrew Lin, F.-K. Hsu, Magnetic iron/carbon nanorods derived from a metal organic framework as an efficient heterogeneous catalyst for the chemical oxidation process in water, RSC Advances, 5 (2015) 50790-50800.

[44] J. Qian, F. Sun, L. Qin, Hydrothermal synthesis of zeolitic imidazolate framework-67 (ZIF-67) nanocrystals, Materials Letters, 82 (2012) 220-223.

[45] R. Banerjee, A. Phan, B. Wang, C. Knobler, H. Furukawa, M. O'Keeffe, O.M. Yaghi, High-Throughput Synthesis of Zeolitic Imidazolate Frameworks and Application to CO2 Capture, Science, 319 (2008) 939-943.

[46] A.F. Gross, E. Sherman, J.J. Vajo, Aqueous room temperature synthesis of cobalt and zinc sodalite zeolitic imidizolate frameworks, Dalton Trans., 41 (2012) 5458-5460.

[47] C.-W. Tang, C.-B. Wang, S.-H. Chien, Characterization of cobalt oxides studied by FT-IR, Raman, TPR and TG-MS, Thermochimica Acta, 473 (2008) 68-73.

[48] M. Kang, M.W. Song, C.H. Lee, Catalytic carbon monoxide oxidation over CoOx/CeO2 composite catalysts, Applied Catalysis A: General, 251 (2003) 143-156.

[49] J. Li, G. Lu, G. Wu, D. Mao, Y. Guo, Y. Wang, Y. Guo, Effect of TiO2 crystal structure on the catalytic performance of Co3O4/TiO2 catalyst for low-temperature CO oxidation, Catalysis Science & Technology, 4 (2014) 1268-1275.

[50] A. Schejn, L. Balan, V. Falk, L. Aranda, G. Medjahdi, R. Schneider, Controlling ZIF-8 nano- and microcrystal formation and reactivity through zinc salt variations, CrystEngComm, 16 (2014) 4493-4500.

[51] N. Liédana, A. Galve, C. Rubio, C. Téllez, J. Coronas, CAF@ZIF-8: One-Step Encapsulation of Caffeine in MOF, ACS Applied Materials & Interfaces, 4 (2012) 5016-5021.

[52] J. Safari, Z. Mansouri Kafroudi, Z. Zarnegar, Co3O4-decorated carbon nanotubes as a novel efficient catalyst in the selective oxidation of benzoins, Comptes Rendus Chimie, 17 (2014) 958-963.

[53] S. Muhammad, E. Saputra, H. Sun, J.d.C. Izidoro, D.A. Fungaro, H.M. Ang, M.O. Tade, S. Wang, Coal fly ash supported Co3O4 catalysts for phenol degradation using peroxymonosulfate, RSC Advances, 2 (2012) 5645-5650.

[54] W. Guo, S. Su, C. Yi, Z. Ma, Degradation of antibiotics amoxicillin by Co3O4-catalyzed peroxymonosulfate system, Environmental Progress & Sustainable Energy, 32 (2013) 193-197.

[55] Y. Yao, Z. Yang, H. Sun, S. Wang, Hydrothermal Synthesis of Co3O4–Graphene for Heterogeneous Activation of Peroxymonosulfate for Decomposition of Phenol, Industrial & Engineering Chemistry Research, 51 (2012) 14958-14965.

[56] J. Shao, Z. Wan, H. Liu, H. Zheng, T. Gao, M. Shen, Q. Qu, H. Zheng, Metal organic frameworks-derived Co3O4 hollow dodecahedrons with controllable interiors as outstanding anodes for Li storage, Journal of Materials Chemistry A, 2 (2014) 12194-12200.

[57] P. Shi, S. Zhu, H. Zheng, D. Li, S. Xu, Supported Co3O4 on expanded graphite as a catalyst for the degradation of Orange II in water using sulfate radicals, Desalination and Water Treatment, 52 (2013) 3384-3391.

[58] A. Rastogi, S.R. Al-Abed, D.D. Dionysiou, Sulfate radical-based ferrous–peroxymonosulfate oxidative system for PCBs degradation in aqueous and sediment systems, Applied Catalysis B: Environmental, 85 (2009) 171-179.

[59] J. Sun, X. Li, J. Feng, X. Tian, Oxone/Co2+ oxidation as an advanced oxidation process: Comparison with traditional Fenton oxidation for treatment of landfill leachate, Water Research, 43 (2009) 4363-4369.

[60] G.S. Toor, M. Lusk, T. Obreza, Onsite Sewage Treatment and Disposal Systems: Trace Organic Chemicals, in: U.I.E. the Soil and Water Science Department (Ed.), UF/IFAS Extension, Gainesville, FL, 2011.

[61] L.A. Schaider, R.A. Rudel, J.M. Ackerman, S.C. Dunagan, J.G. Brody, Pharmaceuticals, perfluorosurfactants, and other organic wastewater compounds in public drinking water wells in a shallow sand and gravel aquifer, Science of The Total Environment, 468–469 (2014) 384-393.

[62] C. Sawyer, P. McCarty, G. Parkin, Chemistry for Environmental Engineering and Science, McGraw-Hill Education, 2003.

[63] K. Liu, J. Lu, Y. Ji, Formation of brominated disinfection by-products and bromate in cobalt catalyzed peroxymonosulfate oxidation of phenol, Water Research, 84 (2015) 1-7.

[64] Z. Li, Z. Chen, Y. Xiang, L. Ling, J. Fang, C. Shang, D.D. Dionysiou, Bromate formation in bromide-containing water through the cobalt-mediated activation of peroxymonosulfate, Water Research, 83 (2015) 132-140.

[65] L.J. Xu, W. Chu, L. Gan, Environmental application of graphene-based CoFe2O4 as an activator of peroxymonosulfate for the degradation of a plasticizer, Chemical Engineering Journal, 263 (2015) 435-443.

Table 1 Kinetic parameters derived from the pseudo first order rate law for the degradation of caffeine using CCN-activated Oxone under various conditions (C_0 of caffeine was fixed to 50 mg L^{-1}).

Conditions					The pseudo first order rate law	
CCN	Oxone	Temp. (°C)	Additive	pH	k_1 (min^{-1})	R^2
25	250	20	−	4	0.0208	0.984
50	250	20	−	4	0.0421	0.970
150	250	20	−	4	0.1000	0.995
50	25	20	−	4	0.0157	0.905
50	150	20	−	4	0.0256	0.962
50	150	30	−	4	0.0520	0.946
50	150	40	−	4	0.1364	0.943
50	150	20	−	3	0.0270	0.963
50	150	20	−	7	0.0104	0.978
50	150	20	−	10	0.0030	0.950
50	150	20	CTAB = 50 mg L^{-1}	4	0.0094	0.967
50	150	20	SDS = 50 mg L^{-1}	4	0.0430	0.970
50	250	20	NaCl = 25 mg L^{-1}	4	0.0290	0.985
50	250	20	NaCl = 150 mg L^{-1}	4	0.0175	0.970
50	250	20	NaCl =250 mg L^{-1}	4	0.0146	0.965
50	250	20	MeOH = 5 wt%	4	0.0011	0.941
50	250	20	TBA = 5 wt%	4	0.0415	0.981

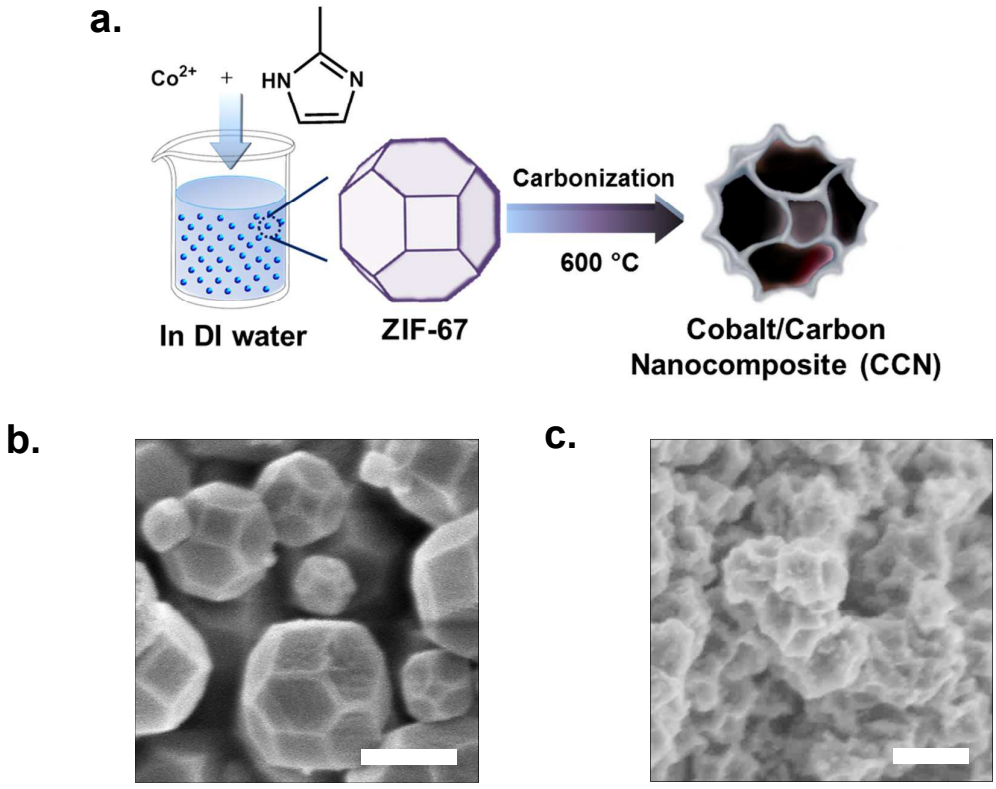

Fig. 1. CCN derived from ZIF-67: **a.** synthesis scheme, **b.** morphology of ZIF-67 and **c.** morphology of CCN. The scale bar is 500 nm.

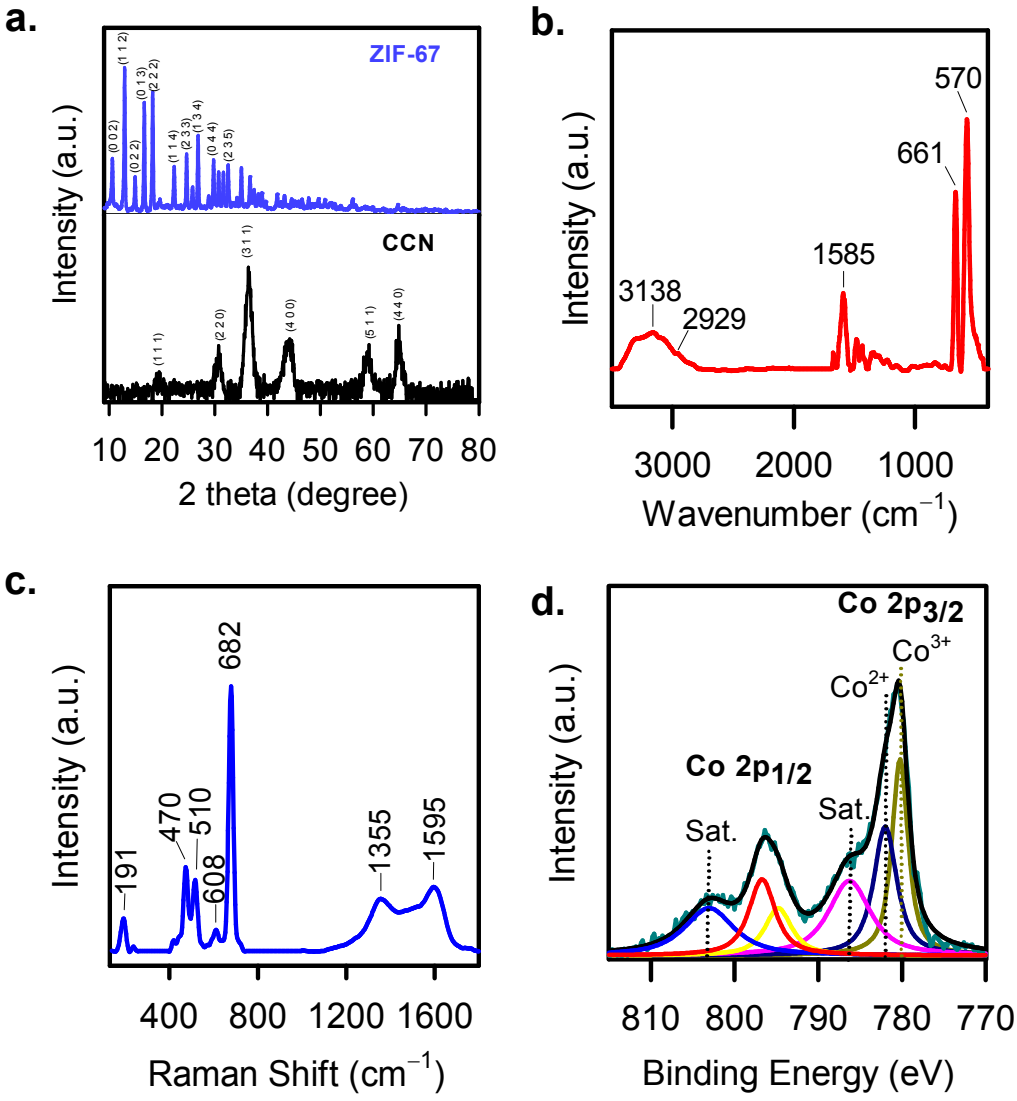

Fig. 2. Characteristics of CCN: **a.** XRD patterns of CCN and its precursor, ZIF-67, **b.** FT-IR spectrum of CCN, **c.** Raman spectrum of CCN and **d.** Co 2p XPS spectrum of CCN.

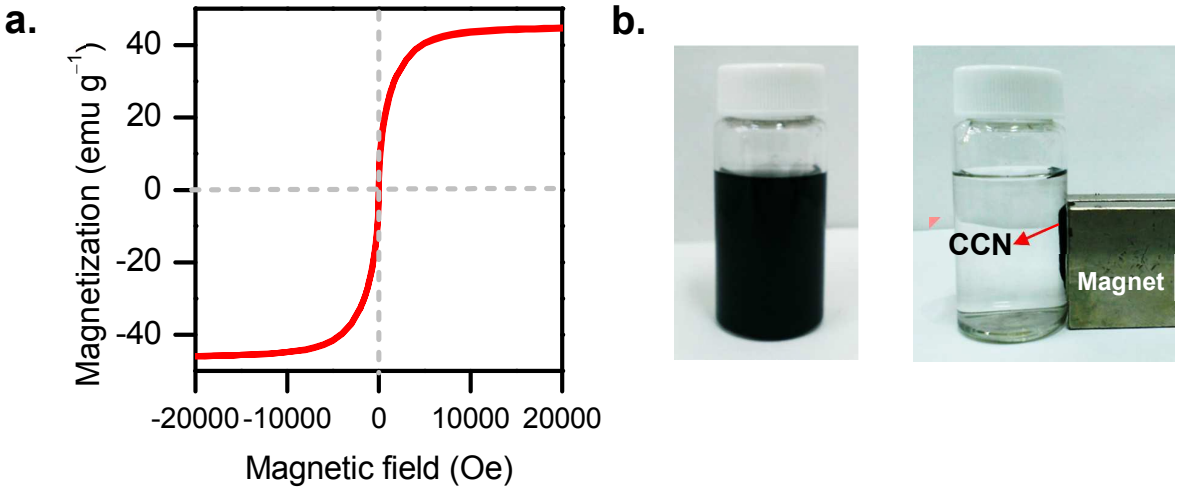

Fig. 3. Magnetic properties of CCN: **a.** saturation magnetization at ambient temperature and **b.** pictures showing that CCN can be magnetically recovered from solutions using an external magnet.

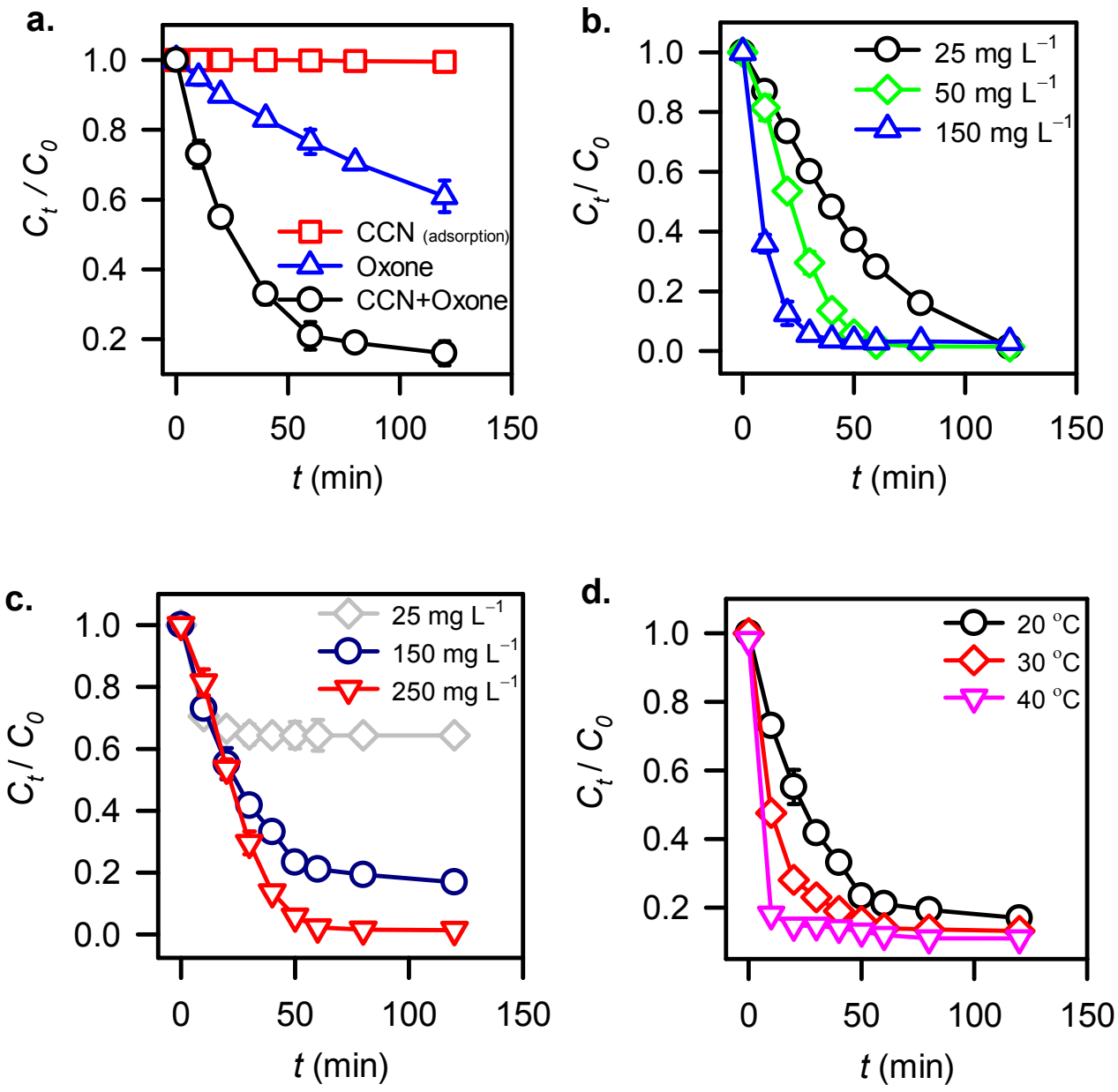

Fig. 4. Elimination of caffeine in water: **a.** comparison between the adsorption to CCN, Oxone alone and CCN/Oxone system (CCN = 50 mg L^{-1}, Oxone = 150 mg L^{-1}, 20 °C) **b.** effect of CCN loading (Oxone = 250 mg L^{-1}, 20 °C), **c.** effect of Oxone dosage (CCN = 50 mg L^{-1}, 20 °C), **d.** effect of temperature (CCN = 50 mg L^{-1}, Oxone = 150 mg L^{-1}).

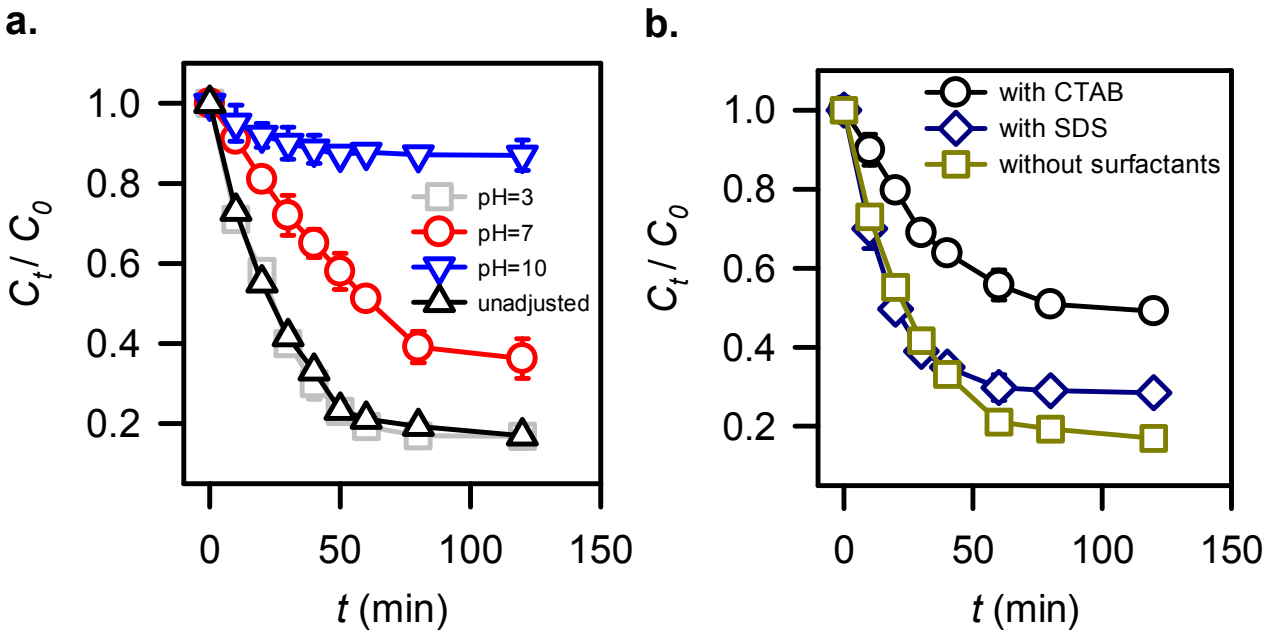

Fig. 5. Effects of **a.** pH and **b.** co-existing surfactants on the elimination of caffeine (CCN = 50 mg L^{-1}, Oxone = 150 mg L^{-1}, 20 °C).

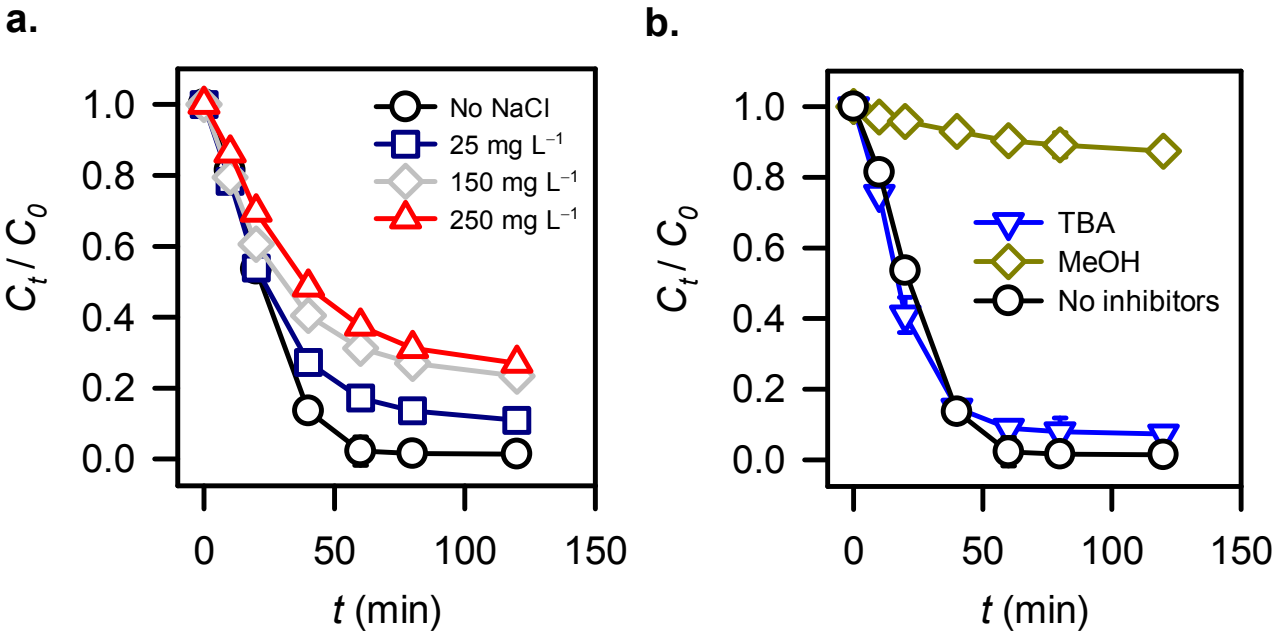

Fig. 6. Effects of **a.** NaCl and **b.** inhibitors on the elimination of caffeine (CCN = 50 mg L^{-1}, Oxone = 250 mg L^{-1}, 20 °C).

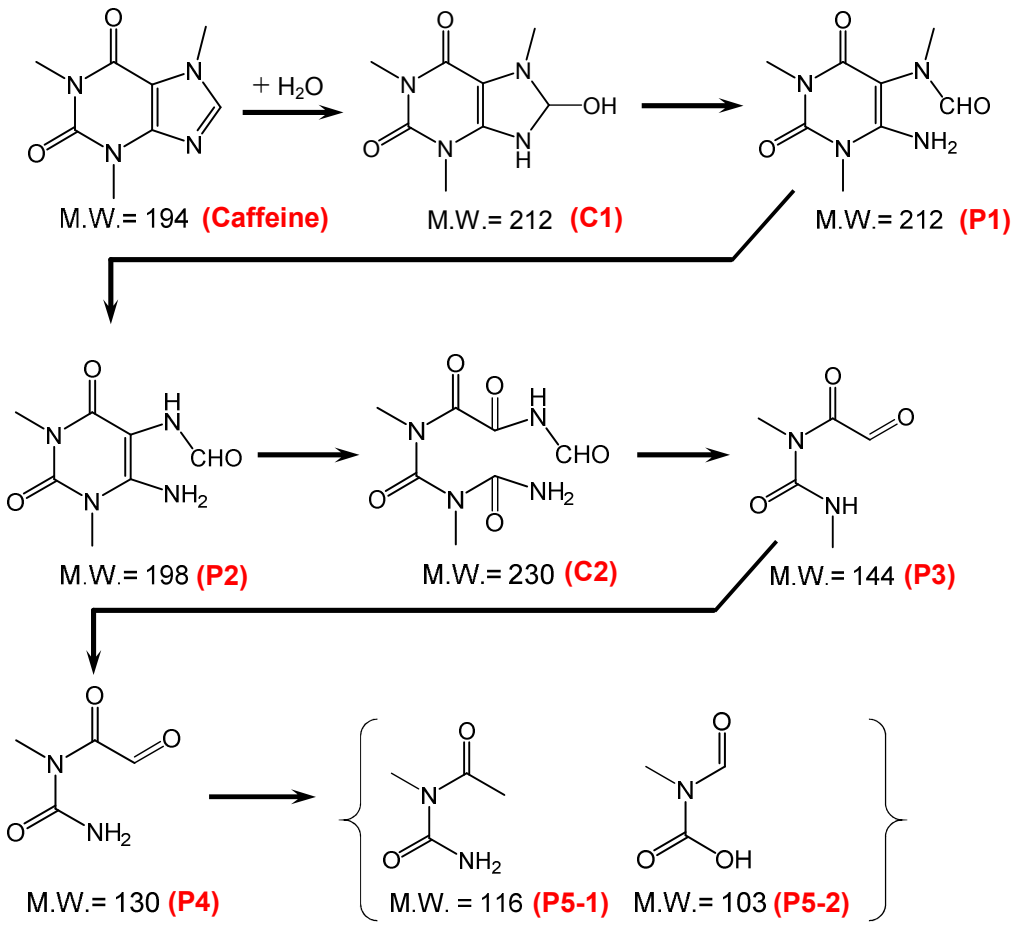

Fig. 7. A proposed degradation pathway of caffeine by CCN-activated Oxone. (P1)-(P5) are intermediates detected in this study using GC-MS.

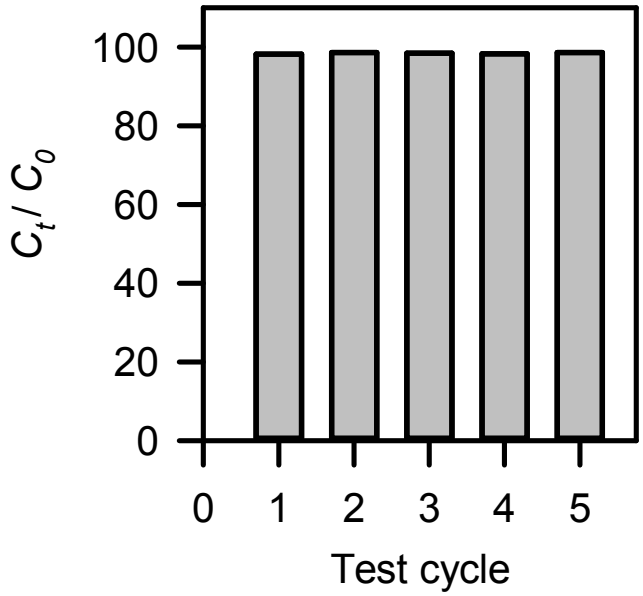

Fig. 8. Recyclability of CCN to activate Oxone for the elimination of caffeine (CCN = 50 mg L^{-1}, Oxone = 250 mg L^{-1}, 20 °C, reaction time = 120 min).